Charge Transfer in Partition Theory[†]

Morrel H. Cohen

Department of Physics and Astronomy, Rutgers University, 126 Frelinghuysen Road, Piscataway, New Jersey 08854, and Department of Chemistry, Princeton University, Washington Road, Princeton, New Jersey 08544

Adam Wasserman*

Department of Chemistry, Purdue University, 560 Oval Drive, West Lafayette, Indiana 47907

Roberto Car

Department of Chemistry and Princeton Institute for the Science and Technology of Materials (PRISM), Princeton University, Princeton, New Jersey 08544

Kieron Burke

Department of Chemistry, University of California at Irvine, 1102 Natural Sciences 2, Irvine, California 92697

Received: September 8, 2008; Revised Manuscript Received: December 9, 2008

The recently proposed partition theory (PT) (*J. Phys. Chem. A* 2007, *111*, 2229.) is illustrated on a simple one-dimensional model of a heteronuclear diatomic molecule, 1D*AB*. It is shown that a sharp definition for the charge of molecular fragments emerges from PT and that the ensuing population analysis can be used to study how charge redistributes during dissociation and the implications of that redistribution for the dipole moment. Interpreting small differences between the isolated parts' ionization potentials as due to environmental inhomogeneities, we gain insight into how electron localization takes place in H_2^+ as the molecule dissociates. Furthermore, by studying the preservation of the shapes of the parts as different parameters of the model are varied, we address the issue of transferability of the parts. We find good transferability within the chemically meaningful parameter regime, raising hopes that PT will prove useful in chemical applications.

1. Introduction

Consider a molecule of composition *AB* with parts *A* and *B* having different ionization potentials when isolated. A long-standing problem is how to associate charges with each part as the parts are separated. At intermediate separations, one expects that, as bonding electrons would spend unequal time in the vicinity of each part, one would have to assign noninteger average numbers of electrons to each, numbers that become integers at infinite separation. Density functional theory (DFT) is defined only for integer electron numbers as originally developed.[1,2] If the dependences of the energy functionals of integer DFT on electron density were continued to densities containing noninteger electron numbers and applied to the separation of *AB* into $A + B$, at infinite separation, *A* and *B* would have unphysical noninteger electron numbers, as pointed out by Perdew et al. (PPLB).[3,4] Instead, PPLB argued that an ensemble generalization of ground-state DFT should be used for systems with noninteger electron numbers.

With how to treat noninteger electron numbers resolved by PPLB, the issue of how rigorously and systematically to decompose a system into its parts remains.[5,6] Two of the present authors have proposed an exact scheme, partition theory (PT),[7−9] based on the PPLB ensemble DFT. In ref 9, their PT was brought to full formal development and used for a reconstruction of chemical reactivity theory, which eliminated the inconsistencies of earlier formulations and enriched them. Applying PT to the case introduced above, $AB \rightarrow A + B$, the parts would obviously be *A* and *B*.

To illustrate the conceptual structure and physical content of PT, a very simple system was studied in ref 10, a caricature of the hydrogen molecule consisting of two electrons moving in one dimension under the influence of two attractive δ-function potentials of equal strength, 1DH_2. Because each part contains in that case exactly one electron for all internuclear separations, invoking the PPLB ensemble was not necessary in ref. 10, thus closely following previous calculations of Guse[11] on H_2 and H_2^+. We obtained analytic solutions for the quantities that he found numerically. In the present paper, a corresponding model of a heteronuclear diatomic molecule *AB* is studied via PT (1D*AB*). The model once again consists of two noninteracting electrons moving in one dimension under the influence of two attractive δ-function potentials of unequal strengths $-Z_A$ and $-Z_B$ with ZB < ZA. Because a one-electron *B*-atom would tend to donate its electron to the more electronegative *A*-atom when brought together, *A* can be thought of as a Lewis acid and *B* as a Lewis base.

In the limit $Z_A = Z_B = Z$, the model becomes that treated in ref 10. Moreover, reducing the number of electrons from two to one requires little modification of that analytic theory, and its numerical results can be used to examine the dependence of charge transfer on $Z_A - Z_B$ and inter"nuclear" separation. The resulting theory can also be used to explore how symmetry breaking localizes the single electron of A_2^+ when it is separated into *A* and A^+, a subtler problem than the localization of both electrons on *A* when $AB \rightarrow A^- + B^+$.

[†] Part of the "Max Wolfsberg Festschrift".

10.1021/jp807967e CCC: $40.75
Published on Web 02/12/2009

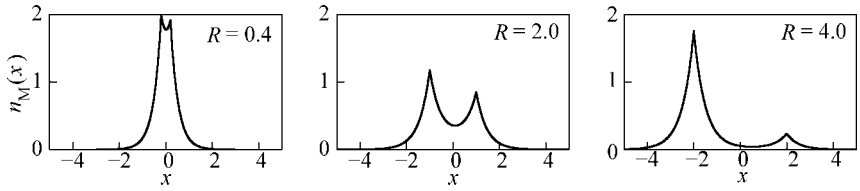

Figure 1. Molecular density for three different internuclear separations: $R = 0.4$ (left), $R = 2.0$ (center), and $R = 4.0$ (right). In this plot, $Z_A = 1.02$, and $Z_B = 0.98$.

In section 2, the formalism developed for the 1DH_2 problem in ref 10 is extended to the present 1DAB problem. Numerical results are given in section 3 for the dependence of the electron densities of the parts, for the charge transfer from A to B, and for the dipole moment as functions of Z_A, Z_B, and the inter "nuclear" separation R. Results are also given there for the partition potential of PT, and how it induces electronegativity equalization between the parts is discussed. The transferability of the properties of the atoms is discussed as well. The united-atom limit, of more academic interest than chemical relevancy, is discussed separately at the end of section 3. Section 4 is devoted to the one-electron molecule 1DAB^+. The case $Z_A \downarrow Z_B$ is used to show how trivial symmetry breaking, $Z_A - Z_B \ll Z_A$, is sufficient to localize the electron on A, illustrating how real H_2^+ separates into $H + H^+$ because of small environmental perturbations. We conclude in section 5 with a brief discussion of the significance of these very simple illustrations of the power and utility of PT for population analysis and for the transferability of fragments with their properties between different molecular contexts. Detailed derivations of all analytic results are presented in an Appendix.

2. 1DAB; Independent Electrons Moving in Unequal δ-Function Potentials in One Dimension

A. The Molecule. In ref 10, we considered an analogue of the H_2 molecule in which two noninteracting electrons move in one dimension under the influence of two δ-function potentials of equal strength $-Z$. In the present section, we consider the heteronuclear analogue 1D AB in which the nuclear δ-function of the acid A is of strength $-Z_A$ and that of the base of strength $-Z_B$, with $Z_A > Z_B$. These "nuclear charges" are allowed to vary continuously. The ground-state wave functions $\psi_\alpha^0(x)$ and energies E_α^0 of the isolated "atoms" $\alpha = A, B$ are (atomic units are used throughout) as follows:

$$\psi_\alpha^0(x) = \sqrt{Z_\alpha}\exp[-Z_\alpha|x|], \tag{2.1}$$

$$E_\alpha^0 = -Z_\alpha^2/2. \tag{2.2}$$

The ground-state energy $E_M(N_M = 1)$ of one electron moving in the two δ-functions, that of strength $-Z_A$ at $x = -R/2$ and that of strength $-Z_B$ at $x = R/2$, is $-\kappa^2/2$, where

$$(\kappa - Z_A)(\kappa - Z_B) = e^{-2\kappa R}Z_A Z_B. \tag{2.3}$$

The solutions of eq 2.3 are plotted as a function of internuclear separation in subsection A of the Appendix. From here on, we are concerned only with the lowest-energy solution, denoted simply as κ, which corresponds to a bonding state that is doubly occupied when $N_M = 2$.

The corresponding ground-state wave function, $\psi_M(x)$, is

$$\psi_M(x) = Ce^{\kappa(R/2+x)},\ x < -R/2,$$

$$= De^{\kappa x} + Fe^{-\kappa x},\ -R/2 < x < R/2,$$

$$= Ge^{\kappa(R/2-x)},\ R/2 < x, \tag{2.4}$$

where C, D, F, and G are constants whose explicit expressions in terms of Z_A, Z_B, R, and κ are given in subsection A of the Appendix (eqs A.1 and A.2). In the combined-atom limit $R \downarrow 0$, $G = C = \kappa^{1/2}$, and D and F are irrelevant. In the limit $R \uparrow \infty$, $C = \kappa^{1/2}$, $D = e^{-\kappa R/2}\kappa^{1/2}$, and $G = F = 0$ so that $\psi_M(x)$ is localized on A only.

The two-electron molecular density is

$$n_M(x) = 2|\psi_M(x)|^2; \tag{2.5}$$

the total energy of the molecule M is

$$E_M(N_M = 2) = 2E_M(N_M = 1) = -\kappa^2; \tag{2.6}$$

and the chemical potential of the molecule is

$$\mu_M = E_M(2) - E_M(1) = -\kappa^2/2, \tag{2.7}$$

all just as for the 1DH_2 case of ref 10. Figure 1 shows the dependence of $n_M(x)$ on internuclear distance R for $Z_A = 1.02$, $Z_B = 0.98$. For these only slightly different values of Z_A and Z_B, the transition from primarily ionic character (right panel) to mixed ionic-covalent character (center panel) occurs at a relatively large bond length $R \sim 3.2$. The left panel of Figure 1 shows a density belonging to the interesting but less chemically meaningful united-atom regime, a regime that we discuss separately in subsection 2D because it allows us to draw conclusions regarding the limits of utility of PT.

B. The Parts. Our task is to partition $n_M(x)$ into contributions from the two parts of M, fragments A and B,

$$n_M(x) = n_A(x) + n_B(x), \tag{2.8}$$

with $n_{A,B}$ localized primarily around $-R/2$, $R/2$, respectively. Because ψ_M and therefore n_M is larger near A than near B (recall that $Z_A > Z_B$), the electron numbers of the fragments,

$$N_{A,B} = \int \mathrm{d}x n_{A,B}(x), \tag{2.9}$$

are unequal with $N_A > N_B$ and

$$N_A + N_B = N_M = 2. \tag{2.10}$$

$N_{A,B}$ are nonintegers in general so that eq 2.1 implies that

$$N_A = 2 - \nu, N_B = \nu, 0 \le \nu \le 1, \tag{2.11}$$

and the PPLB ensemble[3] must be used for the fragments. In this use of the PPLB ensemble lies the main difference with Parr's atoms-in-molecules approach based on a minimum promotion energy criterion.[11] For A, a singly occupied state of either spin occurs with probablility $\nu/2$, and a doubly occupied

state occurs with probability $1 - \nu$ in the PPLB ensemble. For B, an unoccupied state occurs with probability $1 - \nu$ and a singly occupied state of either spin occurs with probability $\nu/2$. The densities of the fragments are, accordingly,

$$n_A(x) = (2 - \nu)\psi_A^2(x), n_B(x) = \nu\psi_B^2(x), \quad (2.12)$$

where $\psi_\alpha(x)$ ($\alpha = A, B$) is a real one-electron wave function localized around $-R/2$, $\alpha = A$, or $+R/2$, $\alpha = B$. Analytic expressions for the $\psi_\alpha(x)$ are derived in subsections B−D of the Appendix. They can be written most simply as:

$$\psi_A(x) = (2 - \nu)^{-1/2}\psi_M(x)[\cos\beta(x) + \sin\beta(x)], \quad (2.13)$$

$$\psi_B(x) = \nu^{-1/2}\psi_M(x)[\cos\beta(x) - \sin\beta(x)], \quad (2.14)$$

where $\beta(x)$ is an auxiliary polar-angle function that determines ν according to

$$\nu = 1 - \int dx\psi_M^2(x)\sin 2\beta(x), \quad (2.15)$$

as shown in detail in subsection B of the Appendix. The corresponding measure of electron transfer q is

$$q = 1 - \nu = \int dx\psi_M^2(x)\sin 2\beta(x) \quad (2.16)$$

In PT, the wave functions and densities of the parts are found by minimizing the sum of the energies of the individual parts subject to the constraints that the electron densities and numbers of the assembly of parts are identical to those of the molecule M. The expressions for $\psi_A(x)$ and $\psi_B(x)$ of eqs 2.13 and 2.14, together with eqs 2.11 and 2.12, guarantee that the constraints are met for 1DAB. Only the determination of $\beta(x)$ remains, and the procedure for determining it by minimizing the sum of the energies of the fragments is described in subsections C and D of the Appendix.

Numerical evaluation of the quantities of interest, ν, $\beta(x)$, and $\psi_\alpha(x)$, is straightforward for representative Z_α and various R. For example, Figure 2 shows the fragments' atomic densities for $Z_A = 1.05$, $Z_B = 0.95$, and $R = 2$. Interestingly, in spite of having high electron density in the bonding region around the molecule's center of mass, the fragment densities resemble true atomic densities. This is one of the most significant results of our work. To investigate the extent to which this is true and to quantify it, results for different parameter regimes are reported and discussed in the next section. First, however, we discuss in the following subsection how the partition potential $v_P(x)$ of PT can be extracted from these results.

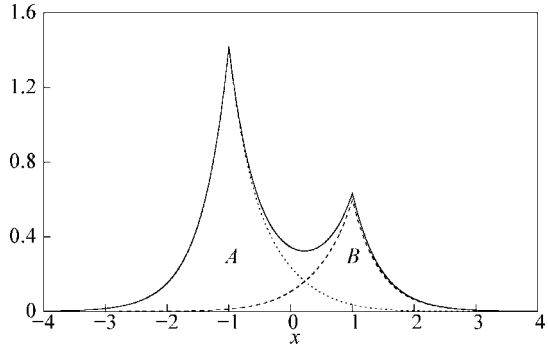

Figure 2. Molecular density $n_M(x)$ (solid), and fragment densities $n_A(x)$ (dotted) and $n_B(x)$ (dashed) for $Z_A = 1.05$, $Z_B = 0.95$, and $R = 2$. For these values, $\nu = 0.6$, indicating substantial charge transfer even with only a 10% difference between Z_A and Z_B and a small R.

C. The Partition Potential. Within the framework of PT,[9] the wave functions $\psi_\alpha(x)$ for the parts $\alpha = A, B$ satisfy the Schrödinger equation

$$[H_\alpha + v_P(x)]\psi_\alpha(x) = \mu_M\psi_\alpha(x), \quad \alpha = A, B, \quad (2.17)$$

where the Hamiltonians H_α for the parts are defined by eq A.11. The partition potential $v_P(x)$ is *the same* for both parts, as is the eigenvalue μ_M, corresponding to the molecular chemical potential, eq 2.7. We construct $v_P(x)$ in subsection E of the Appendix, obtaining:

$$v_P(x) = -\frac{1}{2}\frac{Z_A^2\psi_M^4(-R/2)\cos^2 2\beta_A}{\psi_M^4(x)}\theta(R/2 - |x|) + \frac{1}{2}\sum_\alpha v_\alpha[1 - s_\alpha\tan\beta_\alpha(1 + \cos 2\beta_\alpha)], \quad (2.18)$$

where β_α ($\alpha = A, B$) are constants that determine the upper and lower bounds of $\beta(x)$ (derived in subsection D of the Appendix), $s_\alpha = \pm 1$ (plus sign for part A and minus sign for part B), and $\theta(y)$ (=0 for $y < 0$, =1 for $y > 0$) is the Heaviside step function. Numerical results for $v_P(x)$ are presented and discussed in the next section.

3. Illustrative Results

For purposes of discussion, we define three critical parameters, R_{IP}, R_{den}, and R_{occ}, as the values of R at which significant changes in the ionization potential, the density, and the occupation of a fragment, respectively, take place. Our definitions for R_{IP} and R_{den} are immediately applicable to any diatomic molecule, and our definition for R_{occ} could be easily generalized to be applicable to any diatomic molecule. We start by defining R_{occ} in subsection A to discuss population analysis and charge transfer and continue in subsection B with R_{den} and R_{IP} to address the issue of transferability.

A. Population Analysis; Charge Transfer. First, note that $q = 1 - \nu$ of an electron is transferred from B to A. Figure 3 shows how ν changes when R is varied for four different values of ΔZ (and $\bar{Z} = 1$) for $R > 1$, and Figure 14 does this for smaller R as well. Define R_{occ} as the larger of the two values of R for which $N_A = 2N_B$ (and therefore $\nu = N/3$), a reasonable criterion for the ionic to mixed ionic-covalent crossover. The solid curve in Figure 9 displays the behavior of R_{occ} vs ΔZ. We observe that R_{occ} is a sensitive function of ΔZ, especially as $\Delta Z \to 0$. (We come back to this point in the next paragraph and in section 4 when discussing electron localization in H_2^+ as the molecule dissociates.) This is a simple illustration of the utility of PT to quantify the degree of charge transfer taking place as a heteronuclear diatomic molecule is stretched out. That charge transfer occurs is readily seen from the sequence of molecular

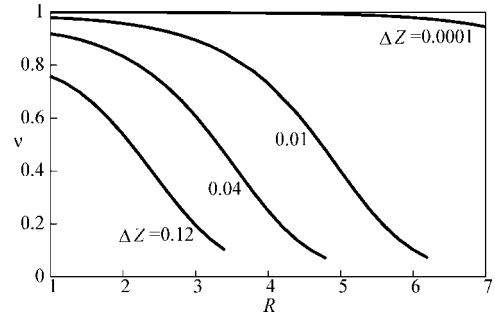

Figure 3. Population of fragment B (=ν) for various values of ΔZ, for $\bar{Z} = 1$.

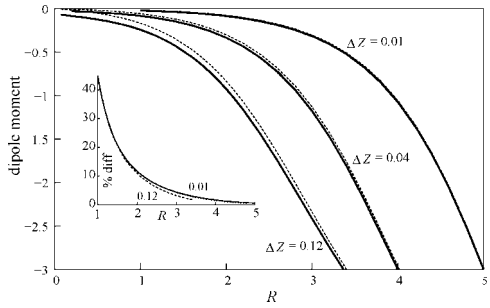

Figure 4. Electronic dipoles as a function of inter "nuclear" separation, both from the point-charge value of eq 3.1 (solid lines), and exactly (dashed) for three different values of ΔZ. The inset shows the absolute percent difference; $\bar{Z} = 1$.

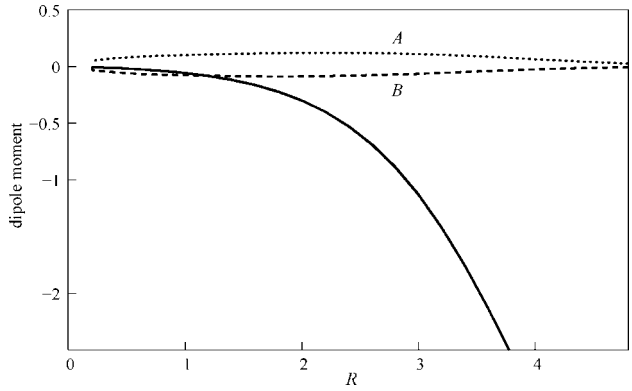

Figure 5. Electronic dipole moment for the 1D*AB* molecule (solid) and fragment dipole moments for fixed $\Delta Z = 0.04$ and $\bar{Z} = 1$.

densities plotted in Figure 1, and PT provides an unambiguous way to characterize it.

This R-dependence of ν is interpretable as a sequence of crossovers in the electronic structure of the molecule M. At large R, M is ionic with $\nu \downarrow 0$ and $q \uparrow 1$. As R decreases, there is a crossover around R_{occ} from that ionic to a mixed ionic-covalent state. As R decreases further, the covalent character of that mixed state increases. At still smaller R, there is another crossover to a combined-atom state around the maximum in ν. Finally, at very small R, there is a rapid crossover back to the ionic state, an interesting fact that we discuss further in subsection E.

It is also of interest to examine how well the product of transferred charge with the internuclear separation agrees with the actual electronic component of the dipole moment of the molecule. Figure 4 compares this point-charge dipole (PC)

$$d_{\mathrm{PC}} = -qR, \tag{3.1}$$

with the actual electronic part of the dipole moment $d = \int dx\, x n_M(x)$ for various values of ΔZ. If the fragment densities were inversion-symmetric about their "nuclei", there would be exact agreement between d_{PC} and d, but there is in addition a dipole moment on each fragment from the polarization of its electron cloud, $d_\alpha = \int dx\, x n_\alpha(x)$, $d = d_{\mathrm{PC}} + d_A + d_B$. Figure 5 shows $d(R)$ along with the fragment dipoles $d_\alpha(R)$, $\alpha = A, B$, for fixed ΔZ. Clearly, when $\Delta Z = 0.04$, the fragment dipoles are small as compared to the molecular dipole only for separations larger than $R \sim 3$. The estimate (eq 3.1) shows excellent agreement whenever the dipole is significant and only fails (error >20%) when the dipole is small (Figure 5). Note also from the inset of Figure 4 that the R-dependence of the percent difference changes little when ΔZ changes from 0.01 to 0.12. Figure 5 shows that d_A is of opposite sign to d_B and d_{PC}. This sign reversal arises

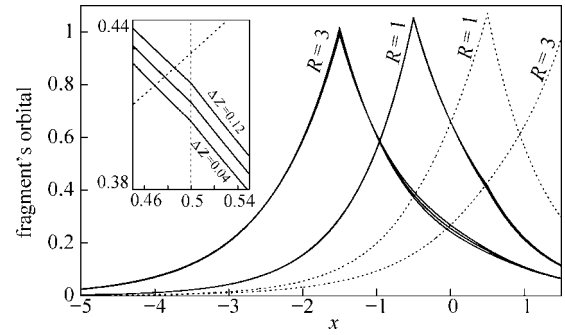

Figure 6. Fragment orbitals $\psi_A(x)$ (solid) and $\psi_B(x)$ (dotted) for different values of R (1 and 3). The fragment-A orbitals are plotted for three different values of ΔZ (0.04, 0.08, and 0.12). Orbitals corresponding to different values of ΔZ start to differ in the overlapping region only for large internuclear separations, $R \gtrsim 3$. Differences due to changes in ΔZ are indistinguishable to the eye for $R \lesssim 3$. The inset zooms in on the $R = 1$ curves around $x = R/2$ to show the cusp present in the A-fragment at the position of the B-"nucleus''.

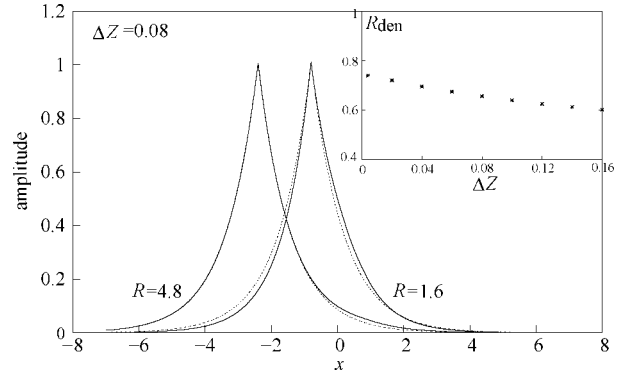

Figure 7. Comparison of fragment orbital $\psi_A(x)$ (solid line) and isolated atomic orbital $\psi_A^0(x)$ (dotted) for $R = 4.8$ and $R = 1.6$. The inset shows the slow variation of R_{den} with ΔZ (see the text).

from the distortion of n_A by covalency, which increases it in the bonding region. However, in 1D*AB*, d_A is not large enough in magnitude to overcome $d_B + d_{\mathrm{PC}}$, even at small R. If it were, d would be of sign opposite to that expected from the electronegativity difference of A and B. In real diatomic molecules containing small bases, such sign reversals are observed,[12] and PT promises a simple explanation.

B. Transferability. The mixed covalent to ionic crossover occurs at quite small R for very small ΔZ when $\bar{Z} = 1$. For the crossover to occur at an internuclear separation of about 1 Å, ΔZ need only be about 0.09. The *shape* of each atom, however, is not as sensitive. Figure 6 shows $\psi_A(x)$ (solid) and $\psi_B(x)$ (dotted) for two different separations and three different values of ΔZ covering the same range as that of Figure 3. It is apparent that orbitals corresponding to different values of ΔZ start differing significantly only close to the region where $\psi_A(x)$ and $\psi_B(x)$ overlap (the "bonding" region) and only for large internuclear separations $R \gtrsim 3$. Because at large internuclear separations the orbitals $\psi_\alpha(x)$ become equal to the isolated solutions $\psi_\alpha^0(x)$ of eq 2.1, it is interesting to examine how and when the $\psi_\alpha(x)$ start departing from the $\psi_\alpha^0(x)$. Figure 7 shows that for $\Delta Z = 0.08$, $\psi_A(x)$ is almost identical to $\psi_A^0(x)$ when $R = 4.8$, differing only slightly in its right-hand tail and that the shape is still preserved for chemically relevant values like $R \sim 1.6$. To appreciate the differences more clearly, Figure 8 displays the differences of the squares $D(x) \equiv \psi_A(x)^2 - [\psi_A^0(x)]^2$. We observe that the two orbitals depart appreciably when the spatial integral of the absolute value of this quantity reaches a value of $\int dx |D(x)| \sim 0.2$, so we define R_{den} as the corresponding

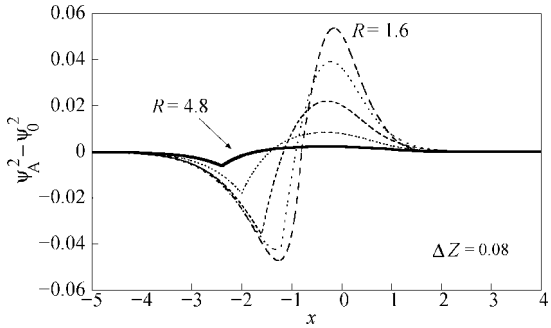

Figure 8. Difference between the fragment density on A and the isolated atomic density, $[(\psi_A^0(x)]^2 - \psi_A^2(x)$, for different values of R (from 1.6 to 4.8 in steps of 0.8) and fixed values of $\Delta Z = 0.08$ and $\bar{Z} = 1$.

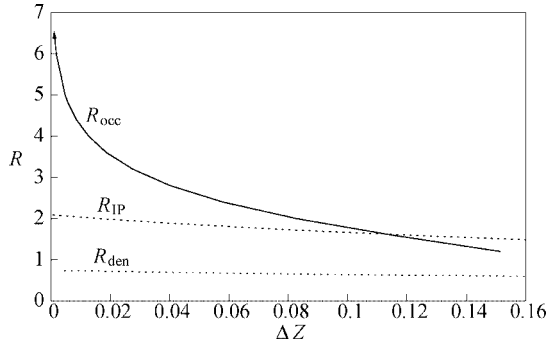

Figure 9. Comparison of R_{occ} (value of R at which the occupation on A is twice the occupation on B), R_{IP} (at which the ionization potential of the molecule is 20% larger than the ionization potential of an isolated A atom), and R_{den} (at which the fragment densities change significantly as compared to the corresponding isolated-atom densities—see the text). All curves with $\bar{Z} = 1$.

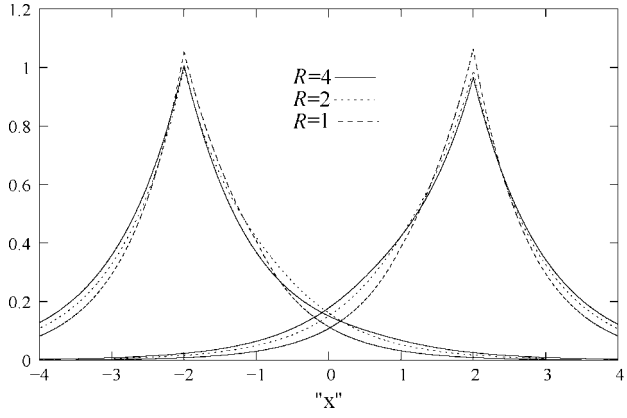

Figure 10. Fragment orbitals $\psi_A(x)$ and $\psi_B(x)$ for $R = 4$ (solid), $R = 2$ (dotted), and $R = 1$ (dashed), when $Z_A = 1.03$ and $Z_B = 0.97$. The A-fragment corresponding to $R = 2$ was shifted to the left by 1 a.u., and the B-fragment was shifted to the right by 1 a.u. The A-fragment corresponding to $R = 1$ was shifted to the left by 1.5 a.u., and the B-fragment was shifted to the right by 1.5 a.u.

separation. As shown in the inset of Figure 7, R_{den} remains almost constant at $R_{den} \sim 0.66$, small as compared to R_{occ} in the corresponding range of ΔZ. A similar behavior is observed for R_{IP}, which we define as the value of R at which the ionization potential of the molecule begins to differ significantly (20%) from the ionization potential of the most electronegative (isolated) atom. Figure 9 compares R_{occ}, R_{IP}, and R_{den}. The preservation of the shape of the orbitals in a range of ΔZ where there is signficant charge transfer ($R_{den} \ll R_{occ}$) is a strong indication of the transferability of the fragments emerging from PT.[13] The feature of transferability can also be seen for fixed

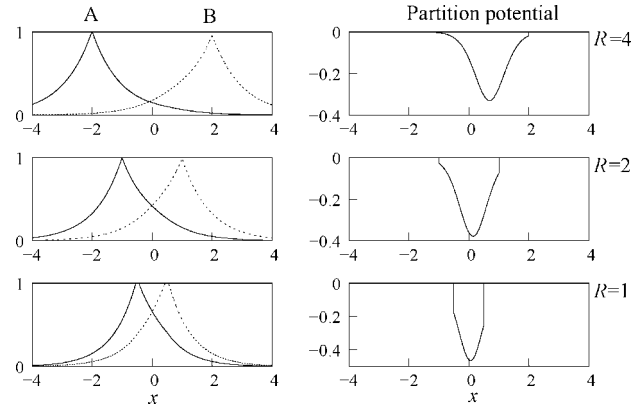

Figure 11. Left panels: A- and B-fragments: $\psi_A(x) = \sqrt{n_A(x)}/(2 - \nu)^{1/2}$ (solid) and $\psi_B(x) = \sqrt{n_B(x)}/\nu^{1/2}$ (dashed) for $R = 4$ (upper), $R = 2$ (center), and $R = 1$ (bottom). Right panels: corresponding partition potentials (δ-functions at $\pm R/2$, not shown). For all of these plots, $Z_A = 1.03$, and $Z_B = 0.97$.

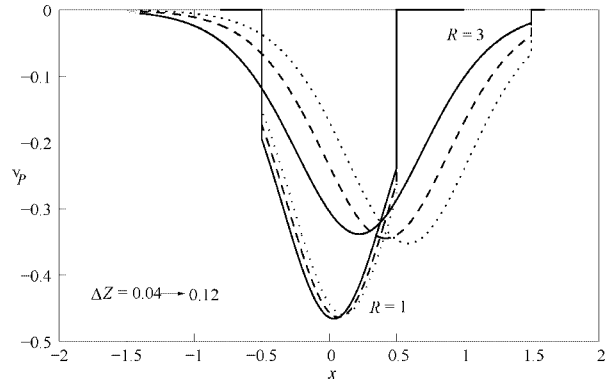

Figure 12. Smooth part of the partition potential for two different values of R and $\Delta Z = 0.04$ (solid), $\Delta Z = 0.08$ (dashed), and $\Delta Z = 0.12$ (dotted). For all of these curves, $\bar{Z} = 1$.

ΔZ by comparing fragments corresponding to different values of R. Figure 10 shows such a comparison for $\Delta Z = 0.06$ by overlapping the $\psi_A(x)$'s corresponding to different R's (this requires shifting the origin of A-atoms to the left and the B-atoms to the right). We note that even though the *size* of the fragments (controlled by ν) changes substantially as R varies from 1 to 4, their shape is quite insensitive to relatively large changes in R with concomitantly large changes in $n_M(x)$ and μ_M. For the value of ΔZ chosen in Figure 10, ν is only about 0.2 when $R = 4$; yet, the shapes of the corresponding fragments only differ slightly from those obtained when $R = 1$ and ν is close to 0.9.

C. Partition Potentials. The corresponding partition potentials are shown in Figure 11. Both parts A and B must have equal electronegativities, sharing the same HOMO eigenvalue, eq 2.17, which must be equal to the overall chemical potential μ_M. The partition potential ensures that this happens by acquiring a specific form, with an asymmetric negative well in between the fragments and two negative δ-functions at $\pm R/2$. In the limit of infinite separation, when $k \rightarrow Z_A$, the external potential of "nucleus'' A does not require any correction in order to reach μ_M, but the external potential of "nucleus" B does. Accordingly, the δ-function component of v_P vanishes on A at infinite separation but *not* on B (Figure 13). It is negative there and has a magnitude smaller than ΔZ because the smooth negative well persists at large separations, getting further from A and closer to B (Figures 11 and 12), thereby contributing to the lowering of the eigen-energy of part B toward μ_M. Figure 12 shows a closer view of the dependence of the smooth part of the partition

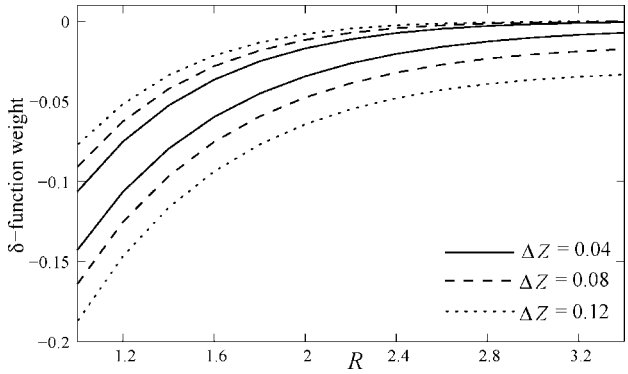

Figure 13. δ-Function weights of the partition potential, for $\Delta Z = 0.04$ (solid), $\Delta Z = 0.08$ (dashed), and $\Delta Z = 0.12$ (dotted). The three upper curves correspond to atom A, and the three bottom ones correspond to atom B. For all of these curves, $\bar{Z} = 1$.

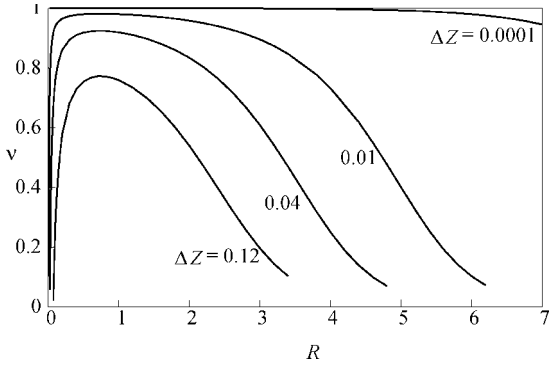

Figure 14. Same as Figure 3 with added small-R range to illustrate striking united-atom behavior of ν (see the text).

potential with ΔZ and with R, and Figure 13 illustrates the same dependences for the amplitudes of its δ-function components.

D. United-Atom Limit. To focus attention on the chemically relevant range of internuclear separations, we started Figure 3 at $R = 1$. The small R behavior of ν can be seen in Figure 14. Perhaps counterintuitively, as R decreases below a given (small) value, a rapid crossover takes place from a mixed ionic-covalent state to an essentially ionic state. In the 1DH_2 model of ref 10, this reversion to the ionic state is absent, the sequence of crossovers being atomic to covalent to combined-atom state. There is a singularity in the 1DAB model at $\Delta Z = 0$, $R = 0$. If $\lim_{R,\Delta Z \downarrow 0}\{(\Delta Z)/(R)\} \downarrow 0$, the combined-atom state persists to $R = 0$. If, however, $\lim_{R,\Delta Z \downarrow 0}\{(R)/(\Delta Z)\} \downarrow 0$, a reversion to the ionic state occurs. This counterintuitive feature illustrates an important limitation to the utility of PT. When κR becomes significantly less than unity as R decreases, the $\psi_\alpha(x)$ overlaps substantially, and the primary motivation of PT, decomposition of the electron density into distinct *localized* components, is frustrated.

The shape of the fragment densities also departs significantly in this limit from pure atomic densities. For example, for the same value of $\Delta Z = 0.08$ used in Figure 8, the maximum value of the difference between $\psi_A(x)^2$ and $\psi_A^0(x)^2$ when $R = 0.4$ is about six times larger than the corresponding maximum when $R = 1.6$.

4. Electron Localization in Dissociating H_2^+

Even though the ground-state wave function of H_2^+ is symmetric, with 50% of its amplitude on the right atom and 50% on the left, the slightest asymmetry due to environmental perturbations forces the electron to localize onto one of the two nuclei as the molecule dissociates. Because this symmetry breaking can now be studied experimentally via intense few-cycle laser pulses with controlled field evolution,[14] there is resurgent interest in theoretical models to describe electron localization during molecular dissociation (see, for example, ref 15 for a recent study of dissociation and ionization of small molecules steered by external noise). Our simple theory of the preceding sections can be used as such a model, provided we interpret small differences between the magnitudes of Z_A and Z_B as due to the effect of an inhomogeneous environment. In fact, because we have dealt with two *noninteracting* electrons, only minor modifications of our results are needed to analyze the one-electron case, 1DAB^+:[16] The chemical potential is still identical to that given by eq 2.7. The number constraint of eq 2.10 is modified to $N_M' = 1$ (we use primed symbols to represent one-electron quantities to distinguish them from their two-electron analogues), and eq 2.11 goes to:

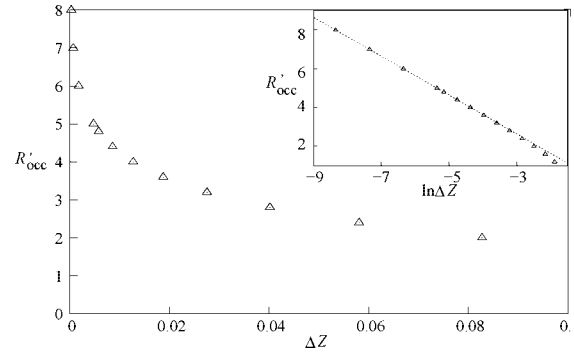

Figure 15. Behavior of $R_{\rm occ}'$ for 1DAB^+ when $\bar{Z} = 1$. The inset shows $R_{\rm occ}'$ vs ln ΔZ. The line corresponds to the best linear fit in the range $-9 \le \ln \Delta Z \le -5$ (slope, -0.185; intercept, -0.502, agreeing with the tight-binding formula derived in the Appendix, eq A.43).

$$N_A' = 1 - \nu', N_B' = \nu', 0 \le \nu' \le \frac{1}{2}. \tag{4.1}$$

The densities of the atoms are

$$n_A'(x) = (1 - \nu')\psi_A^2(x), \quad n_B'(x) = \nu'\psi_B^2(x), \tag{4.2}$$

and following the same steps leading to eq 2.15, we find

$$\nu' = \frac{1}{2}\left[1 - \int \mathrm{d}x\, \psi_M^2(x) \sin 2\beta'(x)\right]. \tag{4.3}$$

Because the Euler equation for $\beta(x)$, eq A.15, as well as the boundary conditions, remain unchanged, $\beta'(x) = \beta(x)$, and the values that ν' takes as a function of R and ΔZ are simply half of those calculated for 1DAB, $\nu' = \nu/2$. As before, we define $R_{\rm occ}'$ as the value of R for which $N_A' = 2N_B'$, corresponding to $\nu' = 1/3$ (from eq 4.1 and $N_A' + N_B' = 1$). The behavior of $R_{\rm occ}'$ as a function of ΔZ is then identical to that of $R_{\rm occ}(\Delta Z)$. The inset of Figure 15 shows that for small ΔZ, $R_{\rm occ}$ is proportional to ln ΔZ. We conclude that the more inhomogeneous the environment (the larger ΔZ), the earlier electron localization occurs along the dissociation pathway, with a logarithmic dependence in this case. As $R_{\rm occ}$ becomes very large when ΔZ becomes small, this striking relation between $R_{\rm occ}$ and ΔZ follows from a simple tight-binding argument outlined in the Appendix (subsection F).

5. Concluding Remarks

We have applied PT[9] to a simple model of a heteronuclear diatomic molecule. We found analytic expressions for the densities of the parts, the charge associated with each of the

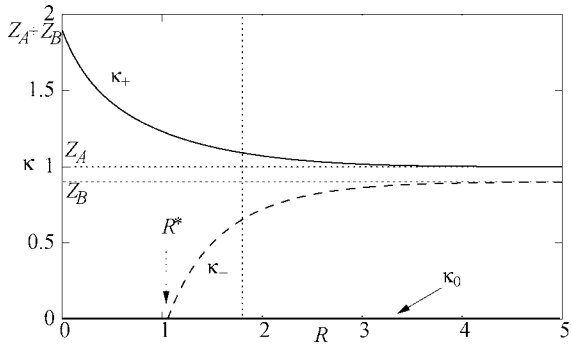

Figure 16. κ vs R for AB with $Z_A = 1$ and $Z_B = 0.9$. The upper curve shows the dependence of κ for the doubly occupied orbital of the ground state, which goes over from ionic on A at infinite R through mixed ionic-covalent to combined-atom at small R. The lower curve shows that of κ for the empty orbital of the excited state, which changes from atomic on B at infinite R to antibonding at intermediate R and disappears for $R < R^*$; $\kappa_0 = 0$ is also a solution of eq 2.3. The vertical dotted line indicates the separation R_{IP} at which κ begins to differ significantly (by 10%) from $\kappa_+(\infty)$.

molecular fragments, and the partition potential that guarantees electronegativity equalization. Numerical calculations for various parameter regimes allow us to reach important conclusions: (1) R_{occ} has a strikingly different bahavior than R_{IP} and R_{den} as $\Delta Z \rightarrow 0$ (Figure 9). Because R_{occ} measures the value of inter-"nuclear" separation at which significant charge transfer occurs and R_{den} and R_{IP} measure the value of R at which signifcant change in the *shape* of the fragment wavefunctions takes place, we conclude that the fragments of PT, at least within this simple model, are to large extent transferrable. (2) Environmental fluctuations (modeled by small finite ΔZ) localize the single electron of H_2^+ onto one of the two nuclei. As H_2^+ dissociates, the more inhomogeneous the environment, the earlier localization occurs along the dissociation pathway. The explicit results reported both here and in ref10 both illustrate important features of PT[9] and support the proposed use of PT for a broad range of applications to real systems, including the sharp definitions of parts of a larger system, population and charge-transfer analysis, and the examination of transferability.

Appendix

A: The Molecule

Equation 2.3 has two solutions for all $R < (Z_A + Z_B)/2Z_AZ_B \equiv R^*$: one, κ_+, belonging to a bonding state doubly occupied when $N = 2$, and another one, $\kappa_0 = 0$, belonging to a state at the bottom of the continuum. For all $R > R^*$, there is another solution, κ_-, corresponding to an unoccupied antibonding state. As $R \uparrow \infty$, κ_+ and κ_- give rise to the two energies $E^0_{A,B}$ of eq 2.2, corresponding to the two states $\psi^0_{A,B}(x)$ of eq 2.1, of which the lower state $\psi^0_A(x)$ localized to the Lewis acid A is doubly occupied, the Lewis base B having donated its electron. As $R \downarrow 0$, κ_+ approaches $Z_A + Z_B$ and gives rise to a doubly occupied combined-atom state with the Z_α of eqs 2.1 and 2.2 replaced by $Z_A + Z_B$. The value of κ_+ decreases monotonically from $Z_A + Z_B$ at $R \downarrow 0$ with finite derivative at zero and vanishing derivative at infinity. κ_- increases monotonically from zero at $R \downarrow R^*$ to Z_B at $R \uparrow \infty$. κ_0 remains zero throughout (see Figure 16). In the text following eq 2.3, we referred only to κ_+, dropping the subscript + for notational simplicity.

The R dependences of all three solutions of eq 2.3 for κ are shown in Figure 16 for $Z_A = 1$ and $Z_B = 0.9$. Note that κ_+ begins to differ significantly from $\kappa_+(\infty)$ only at separation $R < R_{IP} \sim 1.8$, less than relevant for real molecules, except for H_2. For example, for $Z_A = 1$ and $Z_B = 0.9$, one gets from eqs 2.3 and 2.7 an ionization energy equal to that of lithium hydride (LiH), for which the equilibrium bond distance is $R_0 = 3.05$ ($\gg R_{IP}$).

Finally, the constants of eq 2.4 are given in terms of Z_A, Z_B, R, and κ, by:

$$\begin{aligned} D &= e^{\kappa R/2}(1 - Z_A/\kappa)C \\ F &= e^{\kappa R/2}(Z_A/\kappa)C, \\ G &= e^{\kappa R}[(\kappa - Z_A/Z_B)]C \end{aligned} \tag{A.1}$$

$$C = (2\kappa)^{1/2}\left\{\frac{Z_A(\kappa - Z_A)}{Z_B(\kappa - Z_B)}\left(1 + \frac{Z_B^2}{\kappa^2}\right) - \frac{e^{-2\kappa R}Z_A^2}{\kappa^2} + \frac{2Z_A}{\kappa}[1 + 2R(\kappa - Z_A)]\right\}^{-1/2}. \tag{A.2}$$

B: The Polar Angle $\beta(x)$

Substituting eqs 2.12 and 2.5 into eq 2.8 leads to

$$(2 - \nu)\psi_A^2(x) + \nu\psi_B^2(x) = 2\psi_M^2(x). \tag{A.3}$$

Equation A.3 can be rewritten as

$$\chi_A^2(x) + \chi_B^2(x) = \psi_M^2(x), \tag{A.4}$$

where

$$\chi_A(x) = (1 - \nu/2)^{1/2}\psi_A(x),\ \chi_B(x) = (\nu/2)^{1/2}\psi_B(x), \tag{A.5}$$

which permits us to take over the analytic procedures of ref 10. We first rotate $\chi_A(x)$ and $\chi_B(x)$ by $\pi/4$ in the function space in which they are defined, introducing

$$\chi_\pm(x) = \frac{1}{\sqrt{2}}[\chi_A(x) \pm \chi_B(x)] \tag{A.6}$$

and leaving "lengths" within that space invariant so that

$$\chi_+^2(x) + \chi_-^2(x) = \psi_M^2(x). \tag{A.7}$$

Finally, we introduce the polar angle $\beta = \beta(x)$ in the function space,

$$\chi_+(x) = \psi_M(x)\cos\beta(x),\ \chi_-(x) = \psi_M(x)\sin\beta(x), \tag{A.8}$$

$$\chi_{A,B}(x) = \frac{1}{\sqrt{2}}\psi_M(x)[\cos\beta(x) \pm \sin\beta(x)] \tag{A.9}$$

because $\chi_{A,B}(x)$ are non-negative, $|\beta|$ cannot exceed $\pi/4$.

Inserting eq A.9 into eq A.5 and subtracting the squares of the two resulting equations leads to an expression for ν, eq 2.15:

$$\nu = 1 - \int dx\ \psi_M^2(x)\sin 2\beta(x), \tag{A.10}$$

after integrating over x. Determination of the polar angle $\beta(x)$ is thus sufficient for the determination of ν (charge transfer) and the electron population of the fragments (population analysis). For the symmetric $1D H_2$ case, $\beta(x)$ is odd and $\psi_M(x)$ even so that the integral in eq 2.15 vanishes, yielding $\nu = 1$ and equally populated fragments. In the present case, because $\psi_M(x)$ is normalized to unity and $|\sin 2\beta(x)| \leq 1$ with the domain of positive $\beta(x)$ weighted more heavily than that of negative $\beta(x)$, the integral in eq 2.15 lies in (0, 1), as must ν in accordance with eq 2.11.

C: The Euler Equation for $\beta(x)$

In PT,[9] a Hamiltonian is assigned to each part for each integer number of electrons entering into its PPLB ensemble. Because our "electrons" do not interact, it is sufficient to assign a one-electron Hamiltonian to each part,

$$H_\alpha = \frac{p^2}{2} + v_\alpha(x), \quad v_{A,B}(x) = -Z_{A,B}\delta(x \pm R/2). \tag{A.11}$$

The PPLB energy functional of the collection of parts is then

$$\mathcal{E} = (2-\nu)(\psi_A, H_A\psi_A) + \nu(\psi_B, H_B\psi_B)$$

$$= 2[(\chi_A, H_A\chi_A) + (\chi_B, H_B\chi_B)]. \tag{A.12}$$

Inserting the transformation (eq A.9) and the definition (eq A.11) of H_α into eq A.12 results in

$$\mathcal{E} = \int \mathrm{d}x\, \{\psi'^2_M(x) + \psi^2_M(x)[\beta'(x)^2 + v_A(x) + v_B(x) + [v_A(x) - v_B(x)] \sin 2\beta(x)]\} \tag{A.13}$$

for the energy functional $\mathcal{E}$, now a functional only of $\beta(x)$. In eq A.13 and in the following, primes indicate derivatives with respect to x.

Varying $\mathcal{E}$ with respect to $\beta(x)$ yields

$$\delta\mathcal{E} = 2\int \mathrm{d}x\, \psi^2_M(x)\{\beta'(x)\delta\beta'(x) + [v_A(x) - v_B(x)] \cos 2\beta(x)\delta\beta(x)\}. \tag{A.14}$$

The usual integration by parts leads to

$$\delta\mathcal{E} = 2\left\{\psi^2_M(x)\beta'(x)\delta\beta(x)\Big|_{x=-\infty}^{x=\infty} + \int \mathrm{d}x\left[-\frac{\mathrm{d}}{\mathrm{d}x}\left(\psi^2_M(x)\frac{\mathrm{d}\beta(x)}{\mathrm{d}x}\right) + \psi^2_M(x)[v_A(x) - v_B(x)] \cos 2\beta(x)\right]\delta\beta(x)\right\} \tag{A.15}$$

The Euler equation

$$-\frac{\mathrm{d}}{\mathrm{d}x}\left[\psi^2_M(x)\frac{\mathrm{d}\beta(x)}{\mathrm{d}x}\right] + \psi^2_M(x)[v_A(x) - v_B(x)] \cos 2\beta(x) = 0 \tag{A.16}$$

and the boundary conditions

$$\psi^2_M(x)\beta'(x)\delta\beta(x)\Big|_{-\infty}^{\infty} = 0 \tag{A.17}$$

result from imposing stationarity on $\mathcal{E}$. At first glance, it might seem that eq A.17 is satisfied automatically since $\psi^2_M(x) \downarrow 0$ as $|x| \uparrow \infty$. However, unless the boundary condition

$$\beta'(x) = 0, \quad |x| = \infty \tag{A.18}$$

imposed, $\beta'(x)$ diverges unacceptably as $\psi_M^{-2}(x)$ as $|x| \uparrow \infty$.

D: Solving for $\beta(x)$

Because the $v_\alpha(x)$ are δ-function potentials, eq A.16 reduces to

$$\frac{\mathrm{d}}{\mathrm{d}x}\left[\psi^2_M(x)\frac{\mathrm{d}\beta(x)}{\mathrm{d}x}\right] = 0 \tag{A.19}$$

with the additional boundary conditions

$$\left.\begin{aligned} \beta\left(-\tfrac{1}{2}R^+\right) &= \beta\left(-\tfrac{1}{2}R^-\right) \equiv \beta_A \\ \beta'\left(-\tfrac{1}{2}R^-\right) - \beta'\left(-\tfrac{1}{2}R^+\right) &= Z_A \cos 2\beta_A \end{aligned}\right\} x = -\frac{1}{2}R, \tag{A.20}$$

$$\left.\begin{aligned} \beta\left(\tfrac{1}{2}R^-\right) &= \beta\left(\tfrac{1}{2}R^+\right) \equiv \beta_B \\ \beta'\left(\tfrac{1}{2}R^-\right) - \beta'\left(\tfrac{1}{2}R^+\right) &= -Z_B \cos 2\beta_B \end{aligned}\right\} x = \frac{1}{2}R. \tag{A.21}$$

The general solution of eq A.19 is

$$\frac{\mathrm{d}\beta(x)}{\mathrm{d}x} = \frac{\alpha_1}{\psi^2_M(x)}, \tag{A.22}$$

$$\beta(x) = \int^x \mathrm{d}x' \frac{\alpha_1}{\psi^2_M(x')} + \alpha_2, \tag{A.23}$$

with the constants α_1 and α_2 taking on different values in the three domains $|x| > R/2$, $-R/2 < x < R/2$. The condition (eq A.18) implies that α_1 and $\beta'(x)$ vanish for $|x| > R/2$ so that

$$\beta(x) = \beta_A, \; x < -R/2 \text{ and } \beta(x) = \beta_B, \; x > R/2. \tag{A.24}$$

The conditions (eq A.20) and (eq A.21) imply that

$$\alpha_1 = -Z_A\psi^2_M(-R/2) \cos 2\beta_A = -Z_B\psi^2_M(-R/2) \cos 2\beta_B, \; |x| < R/2 \tag{A.25}$$

From eq A.20, α_2 is β_A when the lower limit in eq A.23 is set at $-R/2$, yielding a second relation between β_A and β_B,

$$\beta_B - \beta_A = \alpha_1 \int_{-R/2}^{R/2} \frac{\mathrm{d}x}{\psi^2_M(x)} \tag{A.26}$$

Inserting the explicit form (eq 2.4) for $\psi_M(x)$ into the integral in eq A.26 results in

$$\int_{-R/2}^{R/2} \frac{\mathrm{d}x}{\psi^2_M(x)} = \frac{1}{2\kappa D}\left[\frac{e^{\kappa R/2}}{\psi_M(-R/2)} - \frac{e^{-\kappa R/2}}{\psi_M(R/2)}\right] \tag{A.27}$$

Taken together, eqs A.25−A.27 fix the values of $\beta_{A,B}$, determining $\beta(x)$ for $|x| > R/2$, and eq A.23 then determines $\beta(x)$ for $|x| < R/2$. Figure 17 shows $\beta(x)$ for various values of R and ΔZ, illustrating our qualitative discussion following eq A.10. Charge transfer is associated with the departure of $\beta(x)$ from perfect odd symmetry, as can be seen by direct inspection of eq 2.15. This departure gets more pronounced as R and ΔZ increase,

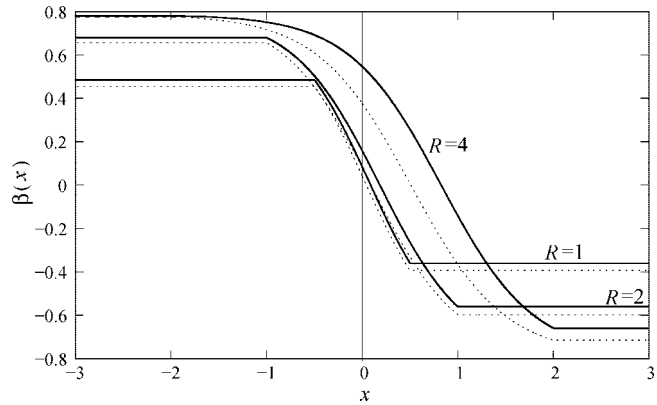

Figure 17. Plot of $\beta(x)$ for three different values of R (1, 2, and 4), and $\Delta Z = 0.04$ (solid) and $\Delta Z = 0.08$ (dashed). For all curves, $\bar{Z} = 1/2(Z_A + Z_B) = 1$.

signaling the transition from covalent to mixed-ionic-covalent character of the chemical bond, as discussed in the text.

E: The Partition Potential

Because the $\chi_\alpha(x)$ is proportional to the $\psi_\alpha(x)$, eq A.5, they satisfy the same Schrödinger equations (eq 2.17). Summing over α and dividing by $\chi_A(x) + \chi_B(x)$ yields

$$v_p(x) = \mu_M - \frac{1}{\chi_A(x)+\chi_B(x)}\frac{p^2}{2}[x_A(x)+x_B(x)] - \frac{v_A(x)\chi_A(x)+v_B(x)\chi_B(x)}{\chi_A(x)+\chi_B(x)}. \quad \text{(A.28)}$$

Expressing $\chi_A(x)$ and $\chi_B(x)$ in terms of $\chi_+(x)$ and $\chi_-(x)$ via eq A.6 and using eq A.8 results in

$$v_P(x) = \mu_M + \frac{1}{2\psi_M(x)\cos\beta(x)}\frac{d^2}{dx^2}[\psi_M(x)\cos\beta(x)] - \frac{1}{2}\sum_\alpha v_\alpha(x)(1+s_\alpha\tan\beta_\alpha), \quad \text{(A.29)}$$

where $s_\alpha = 1$ for $\alpha = A$ and $s_\alpha = -1$ for $\alpha = B$. The δ-function character of $v_\alpha(x)$ and the definitions of β_A and β_B of eqs A.19 and A.20) were also taken into account in arriving at eq A.29. Because the molecular wave function $\psi_M(x)$ satisfies

$$-\frac{1}{2}\frac{d^2\psi_M(x)}{dx^2} + [v_A(x)+v_B(x)]\psi_M(x) = \mu_M\psi_M(x), \quad \text{(A.30)}$$

Equation A.29 can be transformed to

$$v_P(x) = -\frac{1}{2}\left\{\tan\beta(x)\left[\frac{2}{\psi_M(x)}\frac{d\psi_M(x)}{dx}\frac{d\beta(x)}{dx} + \frac{d^2\beta(x)}{dx^2}\right] + \left(\frac{d\beta(x)}{dx}\right)^2\right\} + \frac{1}{2}\sum_\alpha v_\alpha(x)(1-s_\alpha\tan\beta_\alpha). \quad \text{(A.31)}$$

Using the Euler eq A.16 for $\beta(x)$, $v_P(x)$ can be further expressed as

$$v_P(x) = -\frac{1}{2}\left(\frac{d\beta(x)}{dx}\right)^2 + \frac{1}{2}\sum_\alpha v_\alpha(x)[1-s_\alpha\tan\beta_\alpha(1+\cos 2\beta_\alpha)], \quad \text{(A.32)}$$

Finally, by using eqs A.23 and A.25, we note that in the internuclear region $|x| < R/2$, $d\beta(x)/dx$ is simply proportional to $\psi_M^{-2}(x)$, yielding

$$v_P(x) = -\frac{1}{2}\frac{Z_A^2\psi_M^4(-R/2)\cos^2 2\beta_A}{\psi_M^4(x)}\theta(R/2-|x|) + \frac{1}{2}\sum_\alpha v_\alpha[1-s_\alpha\tan\beta_\alpha(1+\cos 2\beta_\alpha)], \quad \text{(A.33)}$$

where $\theta(y)$ (= 0 for $y < 0$ and =1 for $y > 0$) is the Heaviside step function. Equation A.33 correctly reduces to the partition potential of $1DH_2$[10] when $Z_A = Z_B$.

F: Proof That R_{occ} Is Proportional to ln ΔZ for Small ΔZ

We expect that R_{occ}, the nuclear separation at the crossover from covalent to ionic behavior, goes to infinity as $\Delta Z \downarrow 0$. There, the fragment wave functions must approach the free-atom wave functions, and the tight-binding LCAO must be a good approximation to the molecular orbital. We can thus write

$$\psi_M(x) = A\psi_A^0(x) + B\psi_B^0(x) \quad \text{(A.34)}$$

where the $\psi_\alpha^0(x)$ are the orbitals of the isolated atoms, eq 2.1. Taking matrix elements of the molecular Hamiltonian yields equations for A, B, and the molecular energy E_M:

$$[E_A^0 - E_M + v_B^{AA}]A + [(E_B^0 - E_M)S_{AB} + v_A^{AB}]B = 0 \quad \text{(A.35a)}$$

$$[(E_A^0 - E_M)S_{AB} + v_B^{AA}]A + [E_B^0 - E_M + v_A^{BB}]B = 0, \quad \text{(A.35b)}$$

where the E_α^0 are the energies of eq 2.2, $v_{A/B}^{\alpha\beta}$ are matrix elements of the A/B potentials of eq A.11, and S_{AB} is the overlap (ψ_A^0, ψ_B^0). In evaluating all quantities except $E_A - E_M$ and $E_B - E_M$, we can take the limit $\Delta Z \downarrow 0$. The result is

$$S_{AB} = S_{BA} \rightarrow S \sim ZRe^{-ZR}$$
$$v_B^{AA} \rightarrow v_A^{BB} \rightarrow v_d \sim -Z^2e^{-2ZR}$$
$$v_A^{AB} \rightarrow v_B^{BA} \rightarrow v_0 \sim Z^2e^{-ZR}$$

The complete solution of eqs A.35a and A.35b shows that S enters into E_M, A, and B as $1 - S^2$ and Sv_d which become exponentially small corrections as $\Delta Z \downarrow 0$, $R \uparrow \infty$. Similarly v_d enters only in the combination Sv_d and can be neglected as well. Thus the equations for A and B simplify to the classic bonding−antibonding equations

$$(E_A - E_M)A + v_0B = 0 \quad \text{(A.36a)}$$

$$v_0A + (E_B - E_M)B = 0 \quad \text{(A.36b)}$$

The bonding eigenvalue is

$$E_M = \frac{1}{2}(E_A+E_B) - \left\{\left[\frac{1}{2}(E_A-E_B)\right]^2 + v_0^2\right\}^{1/2} \quad \text{(A.37)}$$

and

$$\frac{B}{A} = \frac{E_M - E_A}{V_0} \quad \text{(A.38)}$$

Inserting eq A.37 into eq A.38 and rearranging gives

$$\frac{B}{A} = \sqrt{1+\left(\frac{E_B-E_A}{2v_0}\right)^2} - \left|\frac{E_B-E_A}{2v_0}\right|. \quad \text{(A.39)}$$

Now, because $E_B - E_A = Z\Delta Z$ and $v_0 = -Z^2e^{-ZR}$, then

$$\frac{B}{A} = \sqrt{1+\left(\frac{\Delta Z e^{ZR}}{2Z}\right)^2} - \frac{\Delta Z e^{ZR}}{2Z} \le 1. \quad \text{(A.40)}$$

Thus

$$\frac{B}{A} = f(y) \le 1, \; y \equiv \frac{\Delta Z}{2Z}e^{ZR}$$
$$A = [1+f(y)^2]^{-1/2}$$

The molecular density is

$$n_M(x) = N_M\psi_M(x)^2 = N_M[A^2\psi_A^2(x)^2 + B^2\psi_B^2(x) + 2AB\psi_A(x)\psi_B(x)] = \frac{N_MZ^2}{1+f(y)^2}[g_1(x)+g_2(x)], \quad \text{(A.41)}$$

where

$$g_1(x) = e^{-2Z|x|} + f^2(y)e^{-2Z|x-R|}$$

$$g_2(x) = 2f(y)e^{-Z(|x|+|x-R|)}$$

It can be checked that $g_1(x)$ always exceeds $g_2(x)$ and becomes exponentially larger than $g_2(x)$ as x departs from $(1/2)R - 1/2$ [ln $f(y)$]/Z. The cross term in eq A.41 can then be neglected and $n_M(x)$ is thus of the form obtained from PT: $n_M(x) = N_M A^2 \psi_A(x)^2 + N_M B^2 \psi_B^2(x)$, so that $2A^2$ can be identified with $2 - \nu$ and $2B^2$ can be identified with ν, implying that

$$f^2(y) = \frac{\nu}{N_M - \nu}. \tag{A.42}$$

We have chosen $\nu = N_M/3$ to define R'_{occ}. That implies that $f(y) = 1/\sqrt{2}$ at R'_{occ} for $N_M = 1$ [or $f(y) = 1/\sqrt{5}$ for $N_M = 2$]. This leads to the observed behavior of R'_{occ} in Figure 15:

$$R'_{\mathrm{occ}} = \frac{1}{Z}\ln Z - \frac{1}{Z}\ln(\sqrt{2}\Delta Z) \tag{A.43}$$

Acknowledgment. K.B. and R.C. thank DOE for Grant No. DE-FG02-01ER45928. This paper is in honor of Max Wolfsberg, a dear and valued colleague at UC Irvine. Max was an early pioneer of simple approaches to electronic structure theory in chemistry, especially of 3d transition metals. We hope someday to move from 1d to 3d.

References and Notes

(1) Hohenberg, P.; Kohn, W. *Phys. Rev.* **1964**, *136B*, 864.
(2) Kohn, W.; Sham, L. J. *Phys. Rev.* **1965**, *140*, A1133.
(3) Perdew, J. P.; Parr, R. G.; Levy, M.; Balduz, J. R. *Phys. Rev. Lett.* **1982**, *49*, 1691.
(4) Perdew, J. P. In *Density Functional Methods in Physics*; Dreizler, R. M., da Providencia, J., Eds.; Plenum: New York, 1985; p 265.
(5) Parr, R. G.; Ayers, P. W.; Nalewajski, R. *J. Phys. Chem. A* **2005**, *109*, 3957.
(6) Gázquez, J. L.; Cedillo, A.; Gómez, B.; Vela, A. *J. Phys. Chem. A* **2006**, *110*, 4535.
(7) Cohen, M. H.; Wasserman, A. *Isr. J. Chem.* **2003**, *43*, 219.
(8) Cohen, M. H.; Wasserman, A. *J. Stat. Phys.* **2006**, *125*, 1125.
(9) Cohen, M. H.; Wasserman, A. *J. Phys. Chem. A* **2007**, *111*, 2229.
(10) Cohen, M. H.; Wasserman, A.; Burke, K. *J. Phys. Chem. A* **2007**, *111*, 12447.
(11) Guse, M. P. *J. Chem. Phys.* **1981**, *75*, 828.
(12) Huzinaga, S.; Miyoshi, E.; Sekiya, M. *J. Comput. Chem.* **1993**, *14*, 1440.
(13) Ayers, P. W. *J. Chem. Phys.* **2000**, *113*, 10886.
(14) Kling, M. F.; Siedschlag, Ch.; Verhoef, A. J.; Khan, J. I.; Schultze, M.; Uphues, Th.; Ni, Y.; Uiberacker, M.; Drescher, M.; Krausz, F.; Vrakking, M. J. J. *Science* **2006**, *312*, 246.
(15) Kenfack, A.; Rost, J. M.; Grossmann, F. *New J. Phys.* **2008**, *10*, 013020.
(16) For a detailed study of the one-electron heteronuclear diatomic molecule, HeH^{++}, see Coulson, C. A.; Duncanson, W. E. *Proc. R. Soc. A* **1938**, *165*, 90.

JP807967E